Monthly Notices of the ROYAL ASTRONOMICAL SOCIETY

MNRAS **455,** 618–625 (2016) doi:10.1093/mnras/stv2277

The cluster-scale environment of PKS 2155−304★

E. P. Farina,[1]† M. Fumagalli,[2] R. Decarli[1] and N. Fanidakis[1]

[1]*Max-Planck-Institut für Astronomie, Königstuhl 17, D-69117 Heidelberg, Germany*

[2]*Institute for Computational Cosmology and Centre for Extragalactic Astronomy, Department of Physics, Durham University, South Road, Durham DH1 3LE, UK*

Accepted 2015 September 28. Received 2015 September 22; in original form 2015 August 6

ABSTRACT

PKS 2155−304 is one of the brightest extragalactic source in the X-ray and EUV bands, and is a prototype for the BL Lac class of objects. In this paper, we investigate the large-scale environment of this source using new multi-object as well as long-slit spectroscopy, together with archival spectra and optical images. We find clear evidence of a modest overdensity of galaxies at $z = 0.116\,10 \pm 0.000\,06$, consistent with previous determinations of the BL Lac redshift. The galaxy group has a radial velocity dispersion of 250^{+80}_{-40} km s^{-1} and a virial radius of 0.22 Mpc, yielding a role-of-thumb estimate of the virial mass of $M_{\rm vir} \sim 1.5 \times 10^{13}$ M$_\odot$, i.e. one order of magnitude less than that observed in similar objects. This result hints towards a relatively wide diversity in the environmental properties of BL Lac objects.

Key words: BL Lacertae objects: individual: PKS 2155−304 – galaxies: groups: general.

1 INTRODUCTION

BL Lac objects are a subclass of active galactic nuclei showing a strong, non-thermal variable emission from radio to TeV energies. These properties are usually ascribed to the relativistic jet emission that is closely aligned with the line of sight (Blandford & Rees 1978). Four decades of studies of the host galaxies and of the BL Lacs' close environment have lead to a general consensus that they are mainly hosted by luminous elliptical galaxies embedded in small clusters or group of galaxies (e.g. Weistrop, Smith & Reitsema 1979; Falomo, Melnick & Tanzi 1990; Urry et al. 1993, 2000; Wurtz et al. 1993, 1997; Smith, O'Dea & Baum 1995; Falomo 1996; Falomo & Kotilainen 1999; Scarpa et al. 2000; Nilsson et al. 2008; Kotilainen et al. 2011, see also Falomo, Pian & Treves 2014 for a recent review). Most of these studies are, however, based on photometric data only, and evidence for a rich environment is inferred from the increased number counts of sources in the proximity of the BL Lacs. Only for a handful of objects, the physical association of nearby sources has been further confirmed via dedicated spectroscopy (e.g. Pesce, Falomo & Treves 1994, 1995; Falomo, Pesce & Treves 1995; Lietzen et al. 2008; Muriel et al. 2015).

In this paper, we investigate the close galactic environment of PKS 2155−304, often considered an archetypal of X-ray selected BL Lac objects (Griffiths et al. 1979; Schwartz et al. 1979). It is one of the most luminous, non-transient, extragalactic source known, and it shows a rapid and strong variability in the whole electromagnetic spectrum (e.g. Smith et al. 1992; Sembay et al. 1993; Fan & Lin 2000; Aharonian et al. 2007; Rieger & Volpe 2010; Sandrinelli, Covino & Treves 2014a,b; Zhang et al. 2014). The host of PKS 2155−304 is a luminous elliptical galaxy with $M_{\rm R} = -24.4$ (Falomo et al. 1991; Kotilainen, Falomo & Scarpa 1998) at redshift $z = 0.116$ (Falomo et al. 1993; Sbarufatti et al. 2006[1]). Optical imaging of the field of PKS 2155−304 revealed the presence of a moderate overdensity of galaxies (Falomo et al. 1991, 1993; Wurtz et al. 1997). This finding is corroborated by the detection in high-resolution near-infrared (NIR) images of five galaxies located within ∼20 arcsec (∼40 kpc at $z = 0.116$) from PKS 2155−304 (Liuzzo et al. 2013) and by spectroscopic observations of some of the sources (Falomo et al. 1991, 1993). We here present a comprehensive study of the field of PKS 2155−304 using new spectra gathered with the Magellan Telescope and archival data from Prochaska et al. (2011). This unique data set, including $\gtrsim$34 per cent of all the galaxies brighter than $R = 20$ mag located within 4 arcmin from the BL Lac (see Section 3), will allow us to probe the galactic environment with unprecedented details.

Throughout this paper, we assume a concordance cosmology with $H_0 = 70$ km s^{-1} Mpc^{-1}, $\Omega_{\rm m} = 0.3$ and $\Omega_\Lambda = 0.7$. In this cosmology, at $z = 0.116$, an angular scale of $\Delta\theta = 1$ arcsec corresponds to a proper transverse separation of $R_\perp = 2.1$ kpc. All the quoted magnitudes are expressed in the AB standard photometric system (Oke 1974; Oke & Gunn 1983).

2 TARGET SELECTION, OBSERVATIONS AND DATA ANALYSIS

In this section, we detail the selection of the targets and we present the multi-object and long-slit spectroscopic observations

★ Based on observations undertaken at the 6.5 m Magellan Telescopes.

† E-mail: emanuele.paolo.farina@gmail.com

[1] Spectra available in the ZBLLac archive: http://archive.oapd.inaf.it/zbllac/

© 2015 The Authors
Published by Oxford University Press on behalf of the Royal Astronomical Society

Downloaded from https://academic.oup.com/mnras/article-abstract/455/1/618/984306 by guest on 29 May 2020

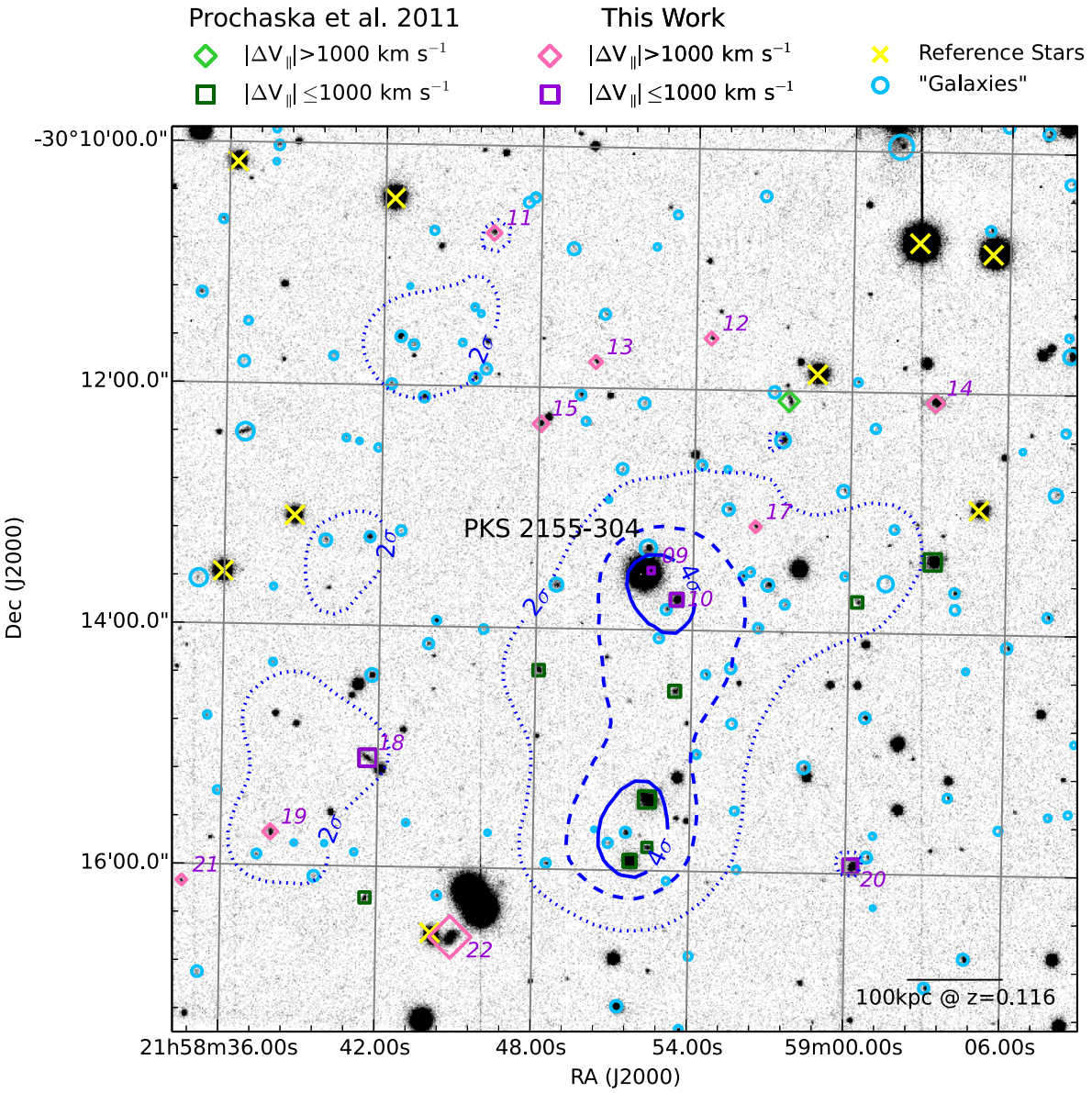


Figure 1. Field of PKS 2155−304 as imaged in the *V* band with EMMI (Falomo, Pesce & Treves 1993, north is up and east is right). Light blue circles mark objects selected as galaxies on the basis of their CLASS_STAR parameter and not confirmed via dedicated spectroscopy. Purple squares and pink diamonds are the targets of multi-object spectroscopy with IMACS. Dark green squares and light green diamonds are archival data from Prochaska et al. (2011). The different shape of the points indicates whether a source is located within ±1000 km s^{-1} from the average redshift of the overdensity (squares) or not (diamonds). The size of the points scales with the effective radius of the objects. Blue dotted, dashed and solid curves are the 2σ, 3σ and 4σ probability level to have an overdensity of galaxy at $z = 0.116$ estimated using the CRS method (see Section 3.1). The nine yellow crosses show the position of the reference stars used for mask alignment.

performed with the Inamori-Magellan Areal Camera and Spectrograph (IMACS; Dressler et al. 2011) mounted on the 6.5 m Magellan Telescope Baade (Las Campanas Observatory, Chile). The data reduction process and the analysis of the spectra are also described. Eventually, we present a summary of the archival photometric and spectroscopic data from Prochaska et al. (2011) used in this work.

2.1 Multi-object spectroscopy

Targets for the multi-object spectroscopy were designated from the analysis of the broad *V*-band image collected by Falomo et al. (1993) with the ESO Multi-Mode Instrument (EMMI; Dekker, Delabre & Dodorico 1986) on the ESO New Technology Telescope (NTT; Fig. 1). The size of this image is 7.5 arcmin × 7.5 arcmin. This roughly corresponds to 950 × 950 kpc^2 at $z = 0.116$, and well fits inside the *f*/4 camera field of view of IMACS (15.4 arcmin × 15.4 arcmin). Data were recalibrated by cross-matching the sources present in the field with the NOMAD catalogue (Zacharias et al. 2004, 2005), reaching an uncertainty on the photometric zero-point of ∼0.1 mag. In order to achieve astrometric accuracy better than 0.5 arcsec on the whole frame (required for mask alignment), the astrometric solution was refined with the ASTROMETRY.NET software (Lang et al. 2010). During the imaging observations, the

Downloaded from https://academic.oup.com/mnras/article-abstract/455/1/618/984306 by guest on 29 May 2020

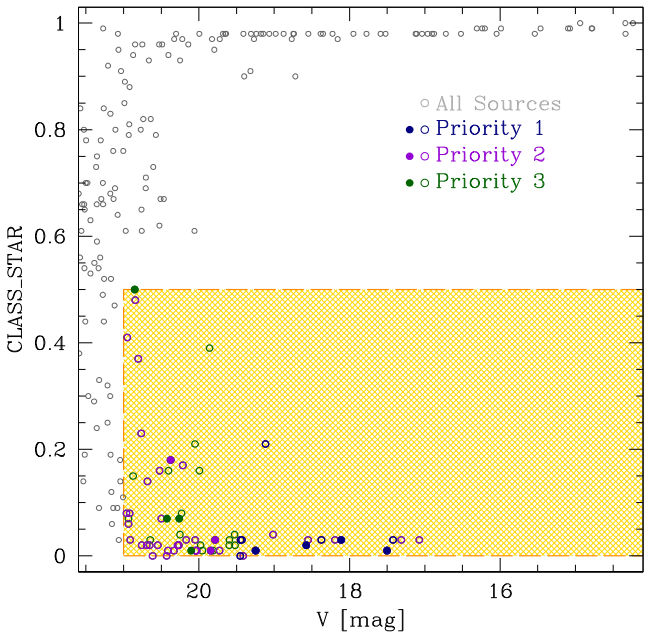


Figure 2. SExtractor star/galaxy classifier (CLASS_STAR) as a function of the apparent *V*-band magnitude of the sources detected in the NTT image. Objects selected for multi-object spectroscopy lie within the yellow hashed region. Different colours of the circles correspond to the priority flag assigned to each target: blue, purple and green for priority 1, 2 and 3, respectively (see Section 2.1 for details). Filled circles are objects spectroscopically observed with IMACS.

seeing was 1.6 arcsec and the reached 5σ detection limit (estimated from the rms of the sky counts integrated within a seeing radius) was $V_{\rm lim} \approx 22.8$ mag.

We used SExtractor (Bertin & Arnouts 1996) to identify and classify sources. An object was considered as a possible target for spectroscopy if its SExtractor star/galaxy classifier (the CLASS_STAR parameter) was smaller than 0.5 (i.e. more likely to be an extended source) and it was brighter than $V = 21$ mag. In Fig. 2, we plot the CLASS_STAR classifier as a function of the *V*-band magnitude. The adopted cut in magnitude allows us to avoid faint sources that SExtractor may fail to classify due their low signal-to-noise in the image. The conservative limit for the CLASS_STAR parameter was chosen to remove the most obvious stars, yet to not miss possible compact galaxies. However, we observe that the majority of the selected sources are in the CLASS_STAR ~ 0 regime. The IMACS mask generation software (maskgen[2]) requires a priority flag to solve conflict between possible overlapping spectra and to maximize the number of sources in the mask. We thus arbitrarily assigned priority 1 (high probability to be included in the mask) to objects with $V < 19.5$ mag and ellipticity $e > 0.2$, priority 2 to those sources with either $V < 19.5$ mag or $e > 0.2$ but not both, and priority 3 to the remaining sources (see Fig. 2). This corresponds to prioritize for bright elliptical galaxies, which are expected to be the dominant population of a putative low-redshift cluster. In addition to this list of targets, we also considered the four galaxies G1, G2, G5 and G6 (following the labels assigned by Falomo et al. 1993 and Liuzzo et al. 2013) observed in high-resolution NIR images by Liuzzo et al. (2013). These sources are positioned at less than ∼20 arcsec from PKS 2155−304 and we assigned them a priority of 1. Eventually, sources from the sample of Prochaska et al. (2011) located outside the NTT image field of view were included with priority of 3. To avoid the gaps between the eight chips of the CCD mosaic (7.7 arcmin × 3.8 arcmin each), we centred our frame 1.5 arcmin north and 1.5 arcmin west from the position of PKS 2155−304 and the mask position angle was set to 270°. 16 apertures of 1 arcsec × 12 arcsec were cut into the mask, corresponding to the targets listed in Table 1 and shown in Fig. 1. In addition, nine reference stars were used for the mask alignment (see Fig. 1).

Multi-object spectroscopy data were gathered on 2013 October 5 using the IMACS grating 300-l. By selecting a central wavelength of 6000 Å, we were able to almost continuously cover the spectral region from ∼3500 to ∼9000 Å (with small variations due to the different positions of the sources). Three contiguous exposures of 1200 s each were collected in clear sky conditions and with an average seeing of ∼0.7 arcsec. The cosmos package[3] was employed for the data reduction. Flux calibration was performed using a spectrum of the standard star Feige 110 acquired during the same night and rescaling the spectra to the *V*-band magnitude of the targets (see Decarli et al. 2008, for further details). Galactic extinction was accounted for according to the map of dust reddening from Schlafly et al. (2014, i.e. $E(B-V) = 0.048$). The reduced spectra typically have a signal-to-noise ratio S/N > 3 per pixel at $\lambda = 6000$ Å and are shown in Fig. S1 in the online version of this paper.

To determine the source redshifts, we followed a three-step procedure. First, we find the redshift (in step of $\Delta z = 0.1$) that best matches each spectrum with the Kinney et al. (1996) galaxy templates rescaled to the magnitude of the target. Then the redshift was refined measuring the position of prominent absorption and emission features and matching them with the line list from the SDSS data set (e.g. Oh et al. 2011). Finally, spectra were independently visually inspected by the authors to verify their redshifts and a quality flag was assigned: $Q_z = 1$ means reliable redshift from apparent emission and/or absorption features, and $Q_z = 2$ means probable redshift. With the exception of PKS 2155−304_22, which seems to show the presence of rest-frame Balmer lines,[4] a redshift was established for all the sources from the measure of two or more features (see Table 1). The uncertainties on the redshifts are typically $\sigma_z \sim 0.0001$.

2.2 Long-slit spectroscopy

In addition to multi-object spectroscopy, we acquired a long-slit spectrum of the two closest galaxies to PKS 2155−304 (i.e. G1 and G5; Falomo et al. 1993; Liuzzo et al. 2013). Data were gathered during the same night of the multi-object spectroscopy with a seeing of ∼0.5 arcsec. Two subsequent exposures of 1500 s each were acquired with the 0.7 arcsec long-slit and the 8.°6 blaze angle of the IMACS grating 600-l, allowing us to nominally cover the wavelength range between 3650 and 6750 Å. The position angle was set to 104° in order to simultaneously collect spectra of both the galaxies and of the BL Lac nebulosity.

[2] http://code.obs.carnegiescience.edu/maskgen

[3] http://code.obs.carnegiescience.edu/cosmos, see also Kelson (2003) for details on the sky subtraction.

[4] We notice that this contaminant lies just at the edge of our selection criteria (see Section 2.1), with $V = 20.85$ and CLASS_STAR = 0.5.

Downloaded from https://academic.oup.com/mnras/article-abstract/455/1/618/984306 by guest on 29 May 2020

Table 1. List of the targets observed with multi-object spectroscopy: our identification label of the object (ID); position (RA, Dec.); *B*, *V* and *R*-band magnitude derived from the NTT image and from Prochaska et al. (2011, *B*, *V*, *R*); angular separation from PKS 2155−304 ($\Delta\theta$); redshift (z); visual inspection quality flag of the determined redshift (Q_z, see the text for details); and alternative label from Falomo et al. (1993) and Prochaska et al. (2011, Alt. ID).

ID	RA (J2000)	Dec. (J2000)	*B* (mag)	*V* (mag)	*R* (mag)	$\Delta\theta$ (arcsec)	z	Q_z	Alt. ID
PKS 2155−304_09	21:58:52.38	−30:13:30.5	–	–	–	4.3	0.1167 ± 0.0001	1	G1[a]
PKS 2155−304_10	21:58:53.33	−30:13:44.6	19.93 ± 0.10	18.55 ± 0.07	18.29 ± 0.06	21.1	0.1166 ± 0.0001	1	G2[a], 1790[b]
PKS 2155−304_11	21:58:46.16	−30:10:43.6	21.32 ± 0.15	20.10 ± 0.13	19.81 ± 0.07	185.1	0.3233 ± 0.0002	2	2085[b]
PKS 2155−304_12	21:58:54.56	−30:11:34.6	21.59 ± 0.15	20.38 ± 0.31	20.21 ± 0.07	122.0	0.2482 ± 0.0003	2	1760[b]
PKS 2155−304_13	21:58:50.13	−30:11:47.1	22.21 ± 0.27	20.26 ± 0.16	19.76 ± 0.07	108.0	0.3119 ± 0.0001	1	1928[b]
PKS 2155−304_14	21:59:03.20	−30:12:05.0	19.29 ± 0.10	18.11 ± 0.33	17.74 ± 0.06	168.5	0.1202 ± 0.0001	1	1389[b]
PKS 2155−304_15	21:58:48.05	−30:12:18.3	21.65 ± 0.21	19.78 ± 0.22	19.14 ± 0.07	90.3	0.3154 ± 0.0001	1	2158[b]
PKS 2155−304_17	21:58:56.36	−30:13:07.8	22.00 ± 0.23	20.42 ± 0.05	19.59 ± 0.07	60.5	0.3127 ± 0.0001	1	1689[b]
PKS 2155−304_18	21:58:41.59	−30:15:05.8	20.75 ± 0.14	19.25 ± 0.63	18.92 ± 0.07	165.1	0.1151 ± 0.0003	2	2210[b]
PKS 2155−304_19	21:58:37.91	−30:15:43.5	21.04 ± 0.14	19.84 ± 0.30	19.36 ± 0.07	225.9	0.2568 ± 0.0001	1	2364[b]
PKS 2155−304_20	21:59:00.21	−30:15:56.2	19.87 ± 0.11	18.57 ± 0.21	18.23 ± 0.06	178.5	0.1157 ± 0.0001	1	1496[b]
PKS 2155−304_21	21:58:34.53	−30:16:08.1	21.80 ± 0.15	20.85 ± 0.06	20.98 ± 0.09	275.8	–	2	2499[b]
PKS 2155−304_22	21:58:44.87	−30:16:34.5	–	17.50 ± 0.52	–	205.1	0.1058 ± 0.0003	2	–
PKS 2155−304_26	21:59:31.12	−30:16:15.0	18.28 ± 0.09	–	16.54 ± 0.06	531.3	0.1154 ± 0.0001	1	351[b]
PKS 2155−304_28	21:59:12.70	−30:11:32.0	19.26 ± 0.09	–	18.20 ± 0.06	292.9	0.1485 ± 0.0001	1	1027[b]
PKS 2155−304_29	21:58:27.60	−30:14:16.0	21.53 ± 0.20	–	19.15 ± 0.07	320.3	0.3137 ± 0.0005	2	2762[b]

Notes. [a] Falomo et al. (1993).
[b] Prochaska et al. (2011).

Standard IRAF[5] procedures for optical spectroscopy were adopted in the data reduction. First, each of the eight detectors of mosaic CCD camera was bias-subtracted and flat-fielded independently. Single exposures were then aligned, combined and cleaned for cosmic rays using the Laplacian edge detection algorithm presented by van Dokkum (2001). The wavelength calibration was applied taking as reference the spectrum of He+Ne+Ar arc lamps.

The small angular separation of PKS 2155−304_09 from PKS 2155−304 causes its spectrum to be embedded within the PKS 2155−304 nebulosity (see Fig. 3). In order to disentangle the two contributions, we make use of our own PYTHON routine. Namely, first the sky emission was removed considering regions free from emission by astrophysical sources. Then, at each pixel of the dispersion axis, we sliced the spectra along the spatial direction and we fitted the profile with a combination of a Gaussian and a Lorentzian function to model the contributions of PKS 2155−304_09 and of the nebulosity, respectively (see Fig. 3). The area subtended by each of the curves was considered as the flux of the sources at that wavelength. The resulting spectra were corrected for Galactic extinction and the achieved signal-to-noise ratios per pixel are typically S/N > 4 at $\lambda = 5500$ Å (see Figs S2 and S3 in the online version of this paper).

The redshifts of the two galaxies were inferred using the method described above (see Table 2), while for the BL Lac object we have first normalized to spectrum with a power law, and then searched for the presence of significant lines (i.e. with an equivalent width greater than $EW_{min} = 1.4$ Å, as estimated using the method of Sbarufatti et al. 2005a). Given this limit, the spectrum does not show the presence of any spectral features. We observe, however, that the redshifted Ca II λλ3934, 3968 and Na D λ5892 lines may be tentatively ($\sim 2\sigma$) detected if the redshift $z = 0.116$ (Falomo et al. 1993; Sbarufatti et al. 2006) is assumed (see Fig. S3 in the electronic version of the journal). Higher signal-to-noise ratio spectra are mandatory to confirm the presence of these features. We point out that these

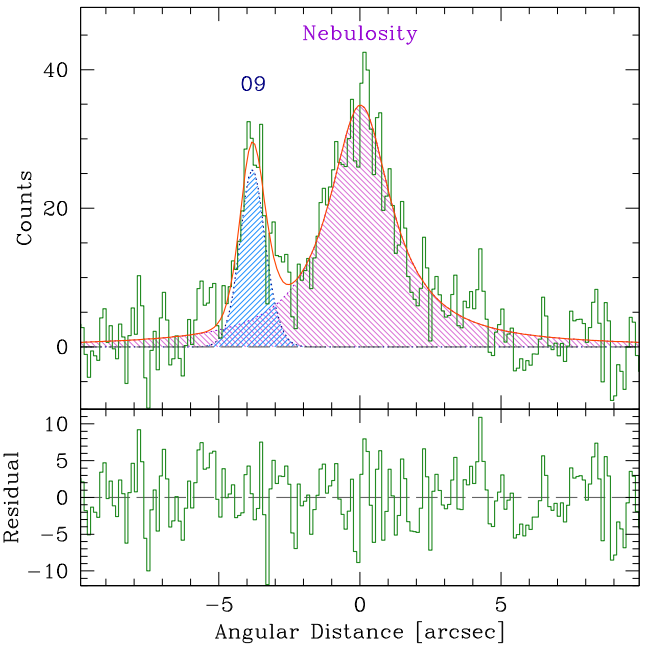


Figure 3. Example of our deblending procedure on a 3 pixel slice of the 2D long-slit spectrum centred at $\lambda = 5500$ Å. Top panel: spatial profile of the two spectra (green line). The contributions of PKS 2155−304_09 and of the PKS 2155−304's nebulosity were deblended performing a simultaneous fit with a Gaussian and a Lorentzian function, respectively (blue and purple shaded areas). The result of the fit is also shown (orange line). Bottom panel: residual spectrum.

[5] IRAF (Tody 1986, 1993) is distributed by the National Optical Astronomy Observatories, which are operated by the Association of Universities for Research in Astronomy, Inc., under cooperative agreement with the National Science Foundation.

Downloaded from https://academic.oup.com/mnras/article-abstract/455/1/618/984306 by guest on 29 May 2020

Table 2. List of targets observed with long-slit spectroscopy: our identification label of the object (ID); position (RA, Dec.); angular separation from PKS 2155−304 ($\Delta\theta$); redshift (z); visual inspection quality flag of the determined redshift (Q_z); and alternative label from Falomo et al. (1993) and Liuzzo et al. (2013, Alt. ID).

ID	RA (J2000)	Dec. (J2000)	$\Delta\theta$ (arcsec)	z	Q_z	Alt. ID
PKS 2155−304_08	21:58:52.63	−30:13:31.4	7.3	0.2008 ± 0.0005	2	G5[a]
PKS 2155−304_09	21:58:52.38	−30:13:30.5	4.3	0.1168 ± 0.0003	1	G1[b]
PKS 2155−304_Neb	21:58:52.13	−30:13:29.6	2.6	–	–	–

Notes. [a] Liuzzo et al. (2013).
[b] Falomo et al. (1993).

absorptions could also arise from the cool gas in the circumgalactic medium of the galaxy group (e.g. Boksenberg & Sargent 1978; Blades, Hunstead & Murdoch 1981; Richter et al. 2011). In this case, the estimates of Falomo et al. (1993) and Sbarufatti et al. (2006) have to be considered as a lower limit for the redshift of PKS 2155−304. The latter scenario is discouraged by the identification of the bright elliptical host galaxy (Falomo 1996; Kotilainen et al. 1998) that could be used as a *standard candle* to determine the redshift (e.g. Sbarufatti, Treves & Falomo 2005b), and by the observation a strong emission of PKS 2155−304 in the TeV regime (Chadwick et al. 1999a,b; Aharonian et al. 2005) that pushes the redshift at $z \ll 1$ due to the interaction of γ-ray photons with the lower frequency photons of the extragalactic background light (see e.g. Aharonian et al. 2013).

2.3 Archival data

To investigate the environment of PKS 2155−304, we also take advantage of the study of Prochaska et al. (2011) aimed to identify galaxies within ∼1 Mpc from ultraviolet bright quasars. In summary: a field of 22 arcmin × 22 arcmin (i.e. 2.7 × 2.7 Mpc^2 at $z = 0.116$) centred on PKS 2155−304 was imaged in the B and R bands with the Swope 40 arcsec telescope in photometric conditions reaching magnitude limits of $B_{\rm lim} \approx 24.0$ mag and $R_{\rm lim} \approx 22.6$ mag. In addition, multi-object spectroscopy of 160 spatially extended sources brighter than $R = 20$ mag was collected using the WFCCD instrument on the du Pont 100-inch telescope (see Prochaska et al. 2011, for further details). We observe that, in the overlapping region between the NTT V-band image and the B- and R-band images from Prochaska et al. (2011), there is a discrepancy on the photometric classification of the sources: employing their cut on the SExtractor star/galaxy classifier (i.e. CLASS_STAR<0.98), ∼30 per cent of the sources we photometrically selected for our multi-object spectroscopic observations (see Section 2.1) are not recognized as 'galaxy' by Prochaska et al. (2011). This is most probably due to the different atmospheric conditions and to subtle difference in the parameters ingested to SExtractor to detect sources in the images. We obtained spectra of four sources that in Prochaska et al. (2011) have CLASS_STAR ≥ 0.98 (i.e. PKS 2155−304_12, PKS 2155−304_13, PKS 2155−304_17 and PKS 2155−304_21), and three of those turn out to be spectroscopically confirmed galaxies. In order to estimate the overdensity of sources around PKS 2155−304 (see Section 3.1), we thus decided to slightly relax the constrain on CLASS_STAR in Prochaska et al. (2011). In the following, we will consider as *galaxies* (based only on the photometric information) objects present in the Prochaska et al. (2011) sample that have CLASS_STAR < 1. This will allow us to recover the missing fraction of galaxies, and, at the same time, to take advantage of the wider sky region covered by the B- and R-band images.

3 RESULTS

Using IMACS multi-object and long-slit spectroscopy we obtained the redshifts of 17 targets in the field of PKS 2155−304. With the exception of PKS 2155−304_22, which possibly presents rest-frame Balmer lines, all the sources are located in the $0.106 \lesssim z \lesssim 0.323$ redshift range (see Tables 1 and 2). Combining these new data with the sample of Prochaska et al. (2011), we reach a completeness in spectroscopy of ∼34 per cent (∼25 per cent) for galaxies brighter than $R = 20$ mag lying within 240 arcsec (600 arcsec) from the BL Lac (see Fig. 4). We stress that, among the sources observed with multi-object spectroscopy, only PKS 2155−304_09 was chosen with a priori knowledge of the redshift. These two samples seem thus well suited for an unbiased study of the galactic environment of PKS 2155−304.

In the following, we will first investigate the environment of PKS 2155−304 using the photometric information only (Section 3.1). Afterwards, e will include the spectroscopic information in our analysis (Section 3.2).

3.1 The overdensity around PKS 2155−304

To verify early suggestions for an overdensity of sources around PKS 2155−304 (Falomo et al. 1991, 1993), we first measured the density of galaxies brighter than $R = 21.08$ mag in different boxes of 5 arcmin × 5 arcmin spread over the field. At the redshift of the BL Lac, this corresponds to cut the luminosity function at $M^\star_{\rm R}+4$ (where $M^\star_{\rm R}$ is the characteristic luminosity of galaxies derived from Blanton et al. 2001). We obtain an average number density of sources of $n_{\rm bkg} = (1.51 \pm 0.07)$ arcmin^{-2} that is lower than what we observed in the box centred on the BL Lac object and $n_{\rm BL\,Lac} = (2.4 \pm 0.3)$ arcmin^{-2}, corresponding to a 3.3σ overdensity. In this estimate, galaxies not present in the *BVR* images (i.e. objects detected only in high-resolution NIR images by Liuzzo et al. 2013) were excluded barring the host galaxy of PKS 2155−304.

Since the *BVR* images considered in this work cover the 4000 Å break at $z \sim 0.116$, we can refine the position and the extent of the overdensity using the cluster red sequence (CRS) method (Gladders & Yee 2000). In summary, we took as reference the red sequence of the Coma cluster (data from the GOLDMine archive;[6] Gavazzi et al. 2003) shifted at $z = 0.116$ using the Kinney et al. (1996) galaxy templates for K- and filter-corrections (see Fig. 4). To each galaxy brighter than $M^\star_{\rm R}+4$, we then assigned a probability to be consistent with the Coma red sequence on the basis of their $B - R$ colours and

[6] http://goldmine.mib.infn.it/

Downloaded from https://academic.oup.com/mnras/article-abstract/455/1/618/984306 by guest on 29 May 2020

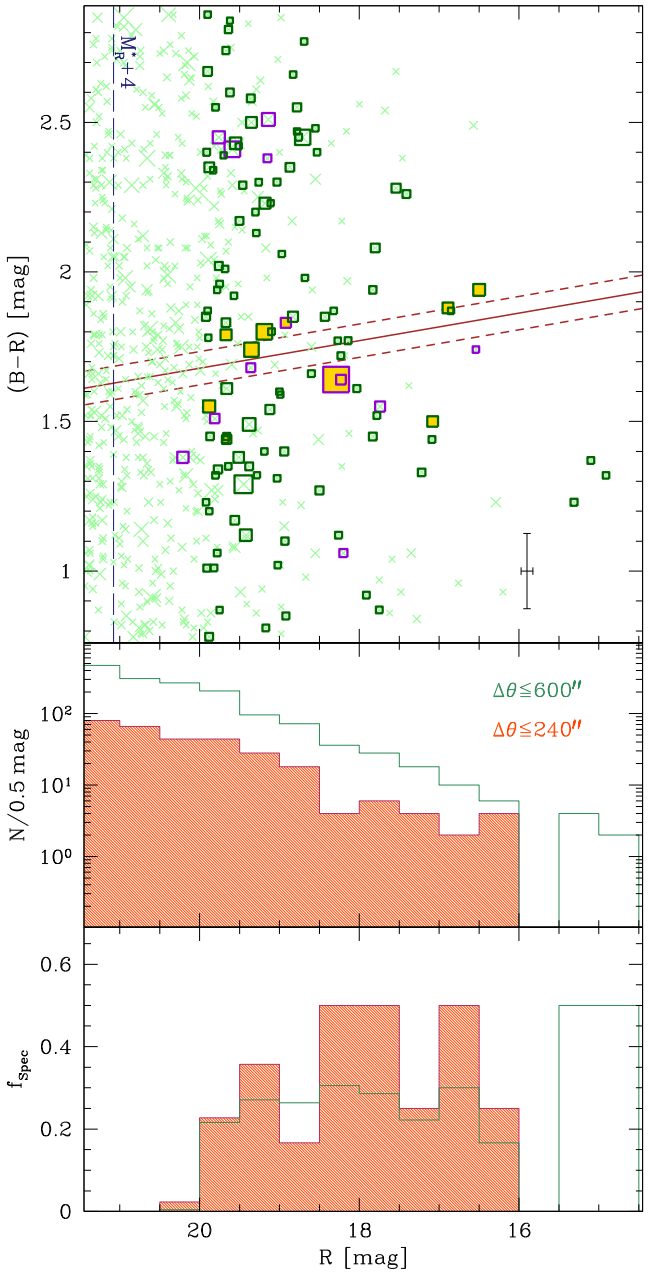


Figure 4. Colour–magnitude diagram of the sources in the field of PKS 2155−304. Galaxies PKS 2155−304_08, PKS 2155−304_09 and the BL Lac host are not detected in the *BVR* images, and are not shown. Top panel: pale green crosses indicate the position of galaxies present in the Prochaska et al. (2011) sample with a size that is proportional to the distance from PKS 2155−304. Framed crosses are targets for which a redshift was determined from our (purple) and Prochaska et al. (2011, dark green) multi-object spectroscopy. Points filled with yellow are targets within 240 arcsec and 1000 km s^{-1} from the BL Lac object. The best fit of Coma cluster red sequence from López-Cruz, Barkhouse & Yee (2004) shifted at the redshift of PKS 2155−304 is also shown (see the text for details). The cross in the bottom right represents typical error bars. Middle panel:number of galaxies per magnitude bin located within 600 arcsec (i.e. ∼1.3 Mpc at $z = 0.116$, green histogram) and 240 arcsec (500 kpc, orange shaded histogram) from PKS 2155−304. Bottom panel: fraction of the sources per magnitude bin for which a redshift is determined spectroscopically. The colour code is the same of the middle panel.

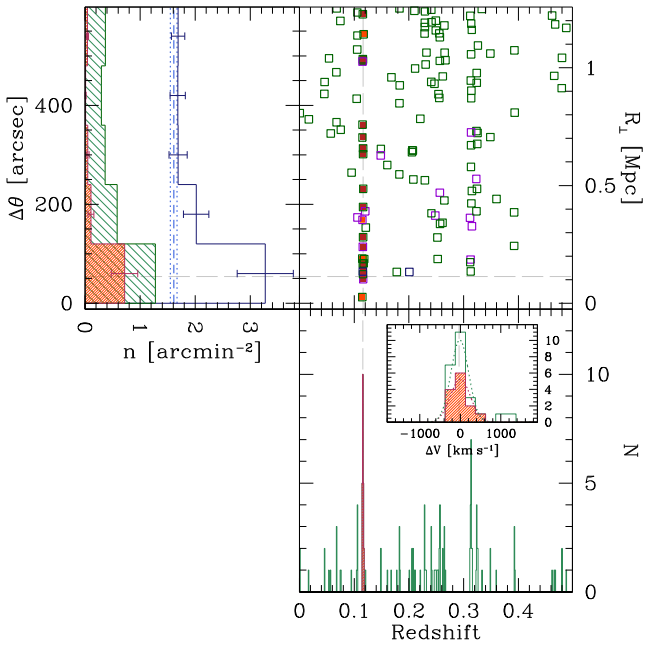


Figure 5. Distribution of the sources in the field of the PKS 2155−304 in the redshift–angular distance from the overdensity peak plane (see Section 3.1). The position of PKS 2155−304 is marked with grey dashed lines. Main panel: green, purple and blue squares are targets with spectra collected by Prochaska et al. (2011), and by our IMACS multi-object and long-slit spectroscopic campaign, respectively. Galaxies with redshift consistent within 1000 km s^{-1} from PKS 2155−304 are marked with filled symbols. Bottom panel – redshift distribution of the sources (green histogram). The inset shows a zoom-in of galaxies within ± 1400 km s^{-1} from PKS 2155−304. Objects located closer than 240 arcsec (i.e. ∼500 kpc at $z = 0.116$) from the peak of the overdensity are highlighted in orange. The best Gaussian fit of the distribution is also shown. Left-hand panel: angular distance distribution of the sources. Galaxies brighter than $R \sim 21$ (i.e. $M_R^\star+4$ at $z = 0.116$) are indicated with the blue histogram. The green shaded histogram indicates sources with redshift determined spectroscopically, and the orange filled one shows the distribution of the sources within ± 1000 km s^{-1} from the BL Lac.

R-band magnitudes. Eventually, a luminosity-weighted probability density was computed using a fixed-kernel smoothing with radius $r_K = 60$ arcsec. In this map, PKS 2155−304 is embedded in a $\gtrsim 4\sigma$ overdensity (see Fig. 1), confirming the evidence that a group of galaxies is associated with the BL Lac.

In order to compare these results with previous works, we measured the galaxy–BL Lac angular cross-correlation function (A_{gb}) and spatial covariance function (B_{gb}; Longair & Seldner 1979) of galaxies brighter that $M_R^\star+2$. This cut in the luminosity function was performed to minimize the uncertainties in B_{gb} (e.g. Yee & López-Cruz 1999) and for consistency with Wurtz et al. (1997). We obtain $A_{gb} = (0.0013 \pm 0.0014)$ rad$^{0.77}$ and $B_{gb} = (80 \pm 79)$ Mpc$^{1.77}$. After correcting for the different cosmologies, these values are smaller than but consistent with the clustering result of Wurtz et al. (1997). This suggests that PKS 2155−304 resides in a small cluster/group of galaxy with an Abell richness class <0.

3.2 Physical properties of the overdensity

In Fig. 5, we present the distribution of objects in the redshift–angular distance plane from the luminosity centre of the group

Downloaded from https://academic.oup.com/mnras/article-abstract/455/1/618/984306 by guest on 29 May 2020

member galaxies, which is located ∼70″ south-east from PKS 2155−304. Considering only sources brighter than M_R^*+4, the decrease of the galaxy density at increasing angular distance is apparent. The redshift distribution of the sources, in bins of $\Delta z = 0.001$, shows a clear peak at $z_g = 0.116\,10 \pm 0.000\,06$, consistent with previous estimates of the redshift of PKS 2155−304, with a nearly Gaussian shape. Assuming that only the 12 galaxies with a spectroscopic redshift within ± 1000 km s^{-1} from z_g (not including the BL Lac host galaxy) and lying within a radius of 240 arcsec (i.e. 500 kpc at $z \sim 0.116$) from the luminosity centre are part of the overdensity, the radial component of the velocity dispersion is $\sigma_\parallel = 250^{+80}_{-40}$ km s^{-1} (where the quoted uncertainties are the 68 per cent confidence level; Danese, de Zotti & di Tullio 1980). Under the hypothesis that the galaxy distribution traces the underlying mass distribution, we used the relations in Girardi et al. (1998) to estimate the virial radius ($R_{vir} \sim 0.22$ Mpc) and the virial mass ($M_{vir} \sim 1.5 \times 10^{13}$ M$_\odot$) of the system. We are cautious to take these estimates as face values. Indeed, for small groups of galaxies, the traditional estimators of the virial radius and mass are not tightly correlated with their real values.

The presence of a second peak at $z \sim 0.314$ indicates that a second overdensity of galaxies may be located ∼40 arcsec north from PKS 2155−304.

4 SUMMARY AND CONCLUSIONS

We investigated the properties of the environment of PKS 2155−304 using broad-band images, new multi-object spectroscopy collected with the IMACS instrument of the Magellan Baade telescope and archival spectra gathered with the du Pont 100-inch telescope by Prochaska et al. (2011). Our measurements confirm that PKS 2155−304 is harboured by a moderate overdensity of galaxies located at $z = 0.116\ 10 \pm 0.000\ 06$, with a virial mass of $M_{vir} \sim 1.5 \times 10^{13}$ M$_\odot$.

To our knowledge, a detailed study of the environment of BL Lac objects with multi-object spectroscopy was performed for only two other targets: RGB 1745+398 ($z = 0.267$; Lietzen et al. 2008) and PKS 0447−439 (with a possible redshift $z = 0.343$; Muriel et al. 2015). Both the sources are found to be associated with large galaxy overdensities with virial masses of few times 10^{14} M$_\odot$. In addition, the detection with *Chandra* of a diffuse X-ray emission, on scales of $\gtrsim$100 kpc, around PKS 0548−322 and PKS 2005−489 suggests that these two BL Lacs are embedded, comparably massive galaxy clusters (Donato et al. 2003). In contrast, the potential presence of gravitational arcs in the *Hubble Space Telescope* images of H 1517+656 ($z = 0.702$;[7] Scarpa et al. 1999) allowed Beckmann et al. (1999) to estimate a virial mass more similar to what we observed for PKS 2155−304: $M_{vir} \sim 1.4 \times 10^{13}$ M$_\odot$. This (small) sample for which the virial mass could be estimated indicates that BL Lac objects are typically hosted by haloes spanning a range of masses, from ∼10^{13} M$_\odot$ to few times 10^{14} M$_\odot$. This suggests that radio-loud sources, in particular BL Lac objects, may be found in a variety (although still massive) galactic environments (see also Wurtz et al. 1997; Lietzen et al. 2011). Although based on a small and heterogeneous sample, it is interesting to put this result in the contest of the current merger-driven paradigm of the nuclear activity (e.g. Barnes & Hernquist 1991; Di Matteo, Springel & Hernquist 2005). In small groups, major mergers between gas-rich galaxies are expected to be frequent and particularly effective in funnelling huge amount of gas in the nuclear regions, eventually triggering the central black hole activity (e.g. Hopkins et al. 2008). Conversely, in rich clusters, the high velocity dispersion decreases the effective cross-section of galaxy interactions, in spite of the higher galaxy densities (e.g. Aarseth & Fall 1980). Galaxy harassment due to high-speed interactions (but not merger) of galaxies could drive dynamical instabilities that efficiently channel gas on to the supermassive black holes in rich environment (Moore et al. 1996). This requires the host galaxy to contain huge gas reservoir. However, ram-pressure stripping is likely to remove the cold gas in cluster galaxies, and the BL Lac hosts are found to be deficient in molecular gas when compared with quasars (e.g. Fumagalli et al. 2012). The trigger mechanism(s) for the nuclear activity of the BL Lac host galaxies is thus likely to be complex and not universal. A larger sample of BL Lac with a detailed characterization of the large-scale environment is thus needed to understand this process in a statistical manner.

[7] The absorption lines used to determine the redshift could belong to an intervening system, rather than to the BL Lac host, so $z = 0.702$ should be considered as a firm lower limit for the redshift of the source (see section 3 in Beckmann, Bade & Wucknitz 1999).

ACKNOWLEDGEMENTS

EPF acknowledges funding through the ERC grant 'Cosmic Dawn'. MF acknowledges support by the Science and Technology Facilities Council, grant number ST/L00075X/1. This paper includes data gathered with the 6.5 m Magellan Telescopes located at Las Campanas Observatory (Chile). We thank J. O'Meara for assisting during observations. EPF is grateful to T. Schmidt, E. Bañados, A. Obreja, M. Fouesneau and C. Ferkinhoff for providing support in the use of PYTHON for the data reduction. We thank A. Treves and R. Falomo for their important contributions to data interpretation and to the shaping of the article. We acknowledge C. Mazzucchelli and M. Landoni for useful comments and suggestions. This research made use of ASTROPY, a community-developed core PYTHON package for Astronomy (Astropy Collaboration 2013) and of APLPY, an open-source plotting package for PYTHON.[8]

REFERENCES

Aarseth S. J., Fall S. M., 1980, ApJ, 236, 43
Aharonian F. et al., 2005, A&A, 430, 865
Aharonian F. et al., 2007, ApJ, 664, L71
Aharonian F., Essey W., Kusenko A., Prosekin A., 2013, Phys. Rev. D, 87, 063002
Astropy Collaboration, 2013, A&A, 558, A33
Barnes J. E., Hernquist L. E., 1991, ApJ, 370, L65
Beckmann V., Bade N., Wucknitz O., 1999, A&A, 352, 395
Bertin E., Arnouts S., 1996, A&AS, 117, 393
Blades J. C., Hunstead R. W., Murdoch H. S., 1981, MNRAS, 194, 669
Blandford R. D., Rees M. J., 1978, Pittsburgh Conference on BL Lac Objects, Some Comments on Radiation Mechanisms in Lacertids. University of Pittsburgh, Pittsburgh, Pa, p. 328
Blanton M. R. et al., 2001, AJ, 121, 2358
Boksenberg A., Sargent W. L. W., 1978, ApJ, 220, 42
Chadwick P. M. et al., 1999a, Astropart. Phys., 11, 145
Chadwick P. M. et al., 1999b, ApJ, 513, 161
Danese L., de Zotti G., di Tullio G., 1980, A&A, 82, 322
Decarli R., Labita M., Treves A., Falomo R., 2008, MNRAS, 387, 1237
Dekker H., Delabre B., Dodorico S., 1986, Proc. SPIE, 627, 339

[8] http://aplpy.github.io/

Downloaded from https://academic.oup.com/mnras/article-abstract/455/1/618/984306 by guest on 29 May 2020

Di Matteo T., Springel V., Hernquist L., 2005, Nature, 433, 604
Donato D., Gliozzi M., Sambruna R. M., Pesce J. E., 2003, A&A, 407, 503
Dressler A. et al., 2011, PASP, 123, 288
Falomo R., 1996, MNRAS, 283, 241
Falomo R., Kotilainen J. K., 1999, A&A, 352, 85
Falomo R., Melnick J., Tanzi E. G., 1990, Nature, 345, 692
Falomo R., Giraud E., Melnick J., Maraschi L., Tanzi E. G., Treves A., 1991, ApJ, 380, L67
Falomo R., Pesce J. E., Treves A., 1993, ApJ, 411, L63
Falomo R., Pesce J. E., Treves A., 1995, ApJ, 438, L9
Falomo R., Pian E., Treves A., 2014, A&AR, 22, 73
Fan J. H., Lin R. G., 2000, A&A, 355, 880
Fumagalli M., Dessauges-Zavadsky M., Furniss A., Prochaska J. X., Williams D. A., Kaplan K., Hogan M., 2012, MNRAS, 424, 2276
Gavazzi G., Boselli A., Donati A., Franzetti P., Scodeggio M., 2003, A&A, 400, 451
Girardi M., Giuricin G., Mardirossian F., Mezzetti M., Boschin W., 1998, ApJ, 505, 74
Gladders M. D., Yee H. K. C., 2000, AJ, 120, 2148
Griffiths R. E., Briel U., Chaisson L., Tapia S., 1979, ApJ, 234, 810
Hopkins P. F., Hernquist L., Cox T. J., Kereš D., 2008, ApJS, 175, 356
Kelson D. D., 2003, PASP, 115, 688
Kinney A. L., Calzetti D., Bohlin R. C., McQuade K., Storchi-Bergmann T., Schmitt H. R., 1996, ApJ, 467, 38
Kotilainen J. K., Falomo R., Scarpa R., 1998, A&A, 336, 479
Kotilainen J. K., Hyvönen T., Falomo R., Treves A., Uslenghi M., 2011, A&A, 534, L2
Lang D., Hogg D. W., Mierle K., Blanton M., Roweis S., 2010, AJ, 139, 1782
Lietzen H., Nilsson K., Takalo L. O., Heinämäki P., Nurmi P., Keinänen P., Wagner S., 2008, A&A, 482, 771
Lietzen H., Heinämäki P., Nurmi P., Liivamägi L. J., Saar E., Tago E., Takalo L. O., Einasto M., 2011, A&A, 535, A21
Liuzzo E. et al., 2013, AJ, 145, 73
Longair M. S., Seldner M., 1979, MNRAS, 189, 433
López-Cruz O., Barkhouse W. A., Yee H. K. C., 2004, ApJ, 614, 679
Moore B., Katz N., Lake G., Dressler A., Oemler A., 1996, Nature, 379, 613
Muriel H., Donzelli C., Rovero A. C., Pichel A., 2015, A&A, 574, A101
Nilsson K., Pursimo T., Sillanpää A., Takalo L. O., Lindfors E., 2008, A&A, 487, L29
Oh K., Sarzi M., Schawinski K., Yi S. K., 2011, ApJS, 195, 13
Oke J. B., 1974, ApJS, 27, 21
Oke J. B., Gunn J. E., 1983, ApJ, 266, 713
Pesce J. E., Falomo R., Treves A., 1994, AJ, 107, 494
Pesce J. E., Falomo R., Treves A., 1995, AJ, 110, 1554
Prochaska J. X., Weiner B., Chen H.-W., Cooksey K. L., Mulchaey J. S., 2011, ApJS, 193, 28
Richter P., Krause F., Fechner C., Charlton J. C., Murphy M. T., 2011, A&A, 528, A12
Rieger F. M., Volpe F., 2010, A&A, 520, A23
Sandrinelli A., Covino S., Treves A., 2014a, A&A, 562, A79
Sandrinelli A., Covino S., Treves A., 2014b, ApJ, 793, L1
Sbarufatti B., Treves A., Falomo R., Heidt J., Kotilainen J., Scarpa R., 2005a, AJ, 129, 559
Sbarufatti B., Treves A., Falomo R., 2005b, ApJ, 635, 173
Sbarufatti B., Falomo R., Treves A., Kotilainen J., 2006, A&A, 457, 35
Scarpa R., Urry C. M., Falomo R., Pesce J. E., Webster R., O'Dowd M., Treves A., 1999, ApJ, 521, 134
Scarpa R., Urry C. M., Falomo R., Pesce J. E., Treves A., 2000, ApJ, 532, 740
Schlafly E. F. et al., 2014, ApJ, 789, 15
Schwartz D. A., Griffiths R. E., Schwarz J., Doxsey R. E., Johnston M. D., 1979, ApJ, 229, L53
Sembay S., Warwick R. S., Urry C. M., Sokoloski J., George I. M., Makino F., Ohashi T., Tashiro M., 1993, ApJ, 404, 112
Smith P. S., Hall P. B., Allen R. G., Sitko M. L., 1992, ApJ, 400, 115
Smith E. P., O'Dea C. P., Baum S. A., 1995, ApJ, 441, 113
Tody D., 1986, Proc. SPIE, 627, 733
Tody D., 1993, in Hanisch R. J., Brissenden R. J. V., Barnes J., eds, ASP Conf. Ser. Vol. 52, Astronomical Data Analysis Software and Systems II. Astron. Soc. Pac., San Francisco, p. 173
Urry C. M. et al., 1993, ApJ, 411, 614
Urry C. M., Scarpa R., O'Dowd M., Falomo R., Pesce J. E., Treves A., 2000, ApJ, 532, 816
van Dokkum P. G., 2001, PASP, 113, 1420
Weistrop D., Smith B. A., Reitsema H. J., 1979, ApJ, 233, 504
Wurtz R., Ellingson E., Stocke J. T., Yee H. K. C., 1993, AJ, 106, 869
Wurtz R., Stocke J. T., Ellingson E., Yee H. K. C., 1997, ApJ, 480, 547
Yee H. K. C., López-Cruz O., 1999, AJ, 117, 1985
Zacharias N., Monet D. G., Levine S. E., Urban S. E., Gaume R., Wycoff G. L., 2004, BAAS, 36, 1418
Zacharias N., Monet D. G., Levine S. E., Urban S. E., Gaume R., Wycoff G. L., 2005, VizieR Online Data Catalog, 1297, 0
Zhang B.-K., Zhao X.-Y., Wang C.-X., Dai B.-Z., 2014, Res. Astron. Astrophys., 14, 933

SUPPORTING INFORMATION

Additional Supporting Information may be found in the online version of this article:

Spectra of the sources collected through multi-object and long-slit spectroscopy are available in the online version of this paper. (http://mnras.oxfordjournals.org/lookup/suppl/doi:10.1093/mnras/stv2277/-/DC1).

Please note: Oxford University Press is not responsible for the content or functionality of any supporting materials supplied by the authors. Any queries (other than missing material) should be directed to the corresponding author for the article.

This paper has been typeset from a TEX/LATEX file prepared by the author.

Downloaded from https://academic.oup.com/mnras/article-abstract/455/1/618/984306 by guest on 29 May 2020